Received: 29 August 2022 | Revised: 20 December 2022 | Accepted: 6 January 2023

DOI: 10.1002/pip.3670

RESEARCH ARTICLE

PROGRESS IN PHOTOVOLTAICS WILEY

In-depth analysis of potential-induced degradation in a commercial CIGS PV module

Pelin Yilmaz[1,2] | Jessica de Wild[3,4,5] | Rémi Aninat[2] | Thomas Weber[6] | Bart Vermang[3,4,5] | Jurriaan Schmitz[1] | Mirjam Theelen[2]

[1]MESA+ Institute for Nanotechnology, University of Twente, Enschede, The Netherlands

[2]TNO partner in Solliance, Eindhoven, The Netherlands

[3]Hasselt University, imo-imomec, Martelarenlaan 42, Hasselt, 3500, Belgium

[4]Imec, imo-imomec, Thor Park 8320, Genk, 3600, Belgium

[5]EnergyVille, imo-imomec, Thor Park 8320, Genk, 3600, Belgium

[6]PI Photovoltaik-Institut Berlin AG, Berlin, Germany

Correspondence
Mirjam Theelen, TNO partner in Solliance, Eindhoven, The Netherlands.
Email: mirjam.theelen@tno.nl

Pelin Yilmaz, MESA+ Institute for Nanotechnology, University of Twente, Enschede, The Netherlands; TNO partner in Solliance, Eindhoven, The Netherlands.
Email: pelinyilmaz88@gmail.com

Jurriaan Schmitz, MESA+ Institute for Nanotechnology, University of Twente, Enschede, The Netherlands.
Email: j.schmitz@utwente.nl

Funding information
TNO; BMWi, Grant/Award Numbers: 0324193B, TEUE116203

Abstract

A post-mortem analysis is conducted after potential-induced degradation (PID) of a commercial copper-indium-gallium-selenide (CIGS) photovoltaic module. After PID, the conversion efficiency of the total module decreased by 62%. Electroluminescence images of the module show that the edges of the modules were much more affected by the PID than the middle part of the module. Coring samples were prepared of the different areas and chemical compositional information of the various areas was combined with electrical characterisation, cell modelling and luminescence data to obtain an overall perspective on the root cause of degradation in these modules during high voltage stress. Consistent with earlier studies on cell level, the module analysis shows the occurrence of alkali migration. From current–voltage modelling, it was concluded that the degradation of the most affected areas is due to an increase in bulk and CdS/CIGS interface defects, likely induced by ion migration. Further degradation on the same samples occurred when they are taken out of the argon-filled glovebox and stored under ambient conditions. Remarkably, the PID-degraded areas show stronger degradation when left in ambient atmosphere, as well as a stronger Na redistribution. These new results show that ion migration not only causes the immediate degradation but also strongly affects the longer-term stability of the cells in ambient atmosphere. This indicates that PID degradation makes CIGS devices more vulnerable to hermeticity problems, which are most prominent at the module edges.

KEYWORDS
CIGS PV, coring, post-mortem analysis, potential-induced degradation

1 | INTRODUCTION

The reliability of photovoltaic (PV) systems is a very important topic, considering the large investments and increasing dependence on PV electricity.[1] In order to obtain the highest possible system reliability, it is crucial to be able to identify, prevent and predict all likely degradation mechanisms.

One common mechanism is 'potential-induced degradation' (PID), which has been observed especially in larger PV systems.[2] In these systems, many modules are series connected to maximise the system voltage, which currently reaches up to 1500 V (positive or negative) and might increase further in the future. These systems are grounded for safety purposes, resulting in high potential differences between the solar cells and the mounting rails and/or grounded frame.

The leakage current that results from these potential differences can take various pathways through and across the module, causing internal potentials that are hard to predict and hard to control.[3] Electric fields thus build up inside the module and may concentrate in specific locations. These internal fields may cause ion drift, electromigration or even local discharges. PID results in the power reduction of a module.[2]

PID has been reported in many PV systems, most commonly for crystalline silicon modules. CIGS devices seem to be less prone to PID: CIGS minimodules have demonstrated higher PID resistance compared to amorphous and multi-crystalline silicon minimodules exposed to the same conditions.[4] Still, some reports of PID occurrence in modules and minimodules are available.[3–7] Actually, PID damage was only reported to occur in the field for the products from one specific CIGS manufacturer. However, future larger PV systems could have maximum system voltages exceeding +/−1500 V, resulting in higher risks on PID. It is therefore important to study, understand and, if necessary, mitigate the degradation mechanisms that can occur for PID in CIGS PV systems.

The dominant PID mechanisms in crystalline silicon PV are shunting due to sodium incorporation at stacking faults and surface polarisation.[8,9] These mechanisms are not expected or even impossible in thin-film multi-crystalline CIGS devices. For these devices, other root causes for the performance loss have been proposed, which include TCO corrosion and pn junction damage.[4,10] However, a complete understanding of the mechanisms causing PID in CIGS modules is still lacking. One reason for the incomplete understanding of PID is the poor connection between laboratory and field studies. Field studies often focus on full-scale modules that have degraded in the field: Analysis mainly focuses on macroscopic properties, like the current–voltage data, leakage current measurements and electroluminescence imaging. Hampered by the packaging of the modules, including encapsulant materials and front- and backsheets, studies do not report on the (microscopic) cell and material properties of the degraded modules. Therefore, only limited information on the root causes and degradation mechanisms can be obtained.

On the other hand, laboratory produced CIGS cells and minimodules allow in-depth microanalysis. Based on such studies, sodium migration from the substrate and accumulation in (among others) the pn junction have been reported.[10] Although this aids the identification of degradation mechanisms behind PID, both the samples and the exposure conditions are dissimilar to modules in the field. Also, the areas of laboratory cells and modules are orders of magnitude smaller. Cell areas are usually smaller than 1 cm^2 and minimodules about 5 × 5 or 10 × 10 cm^2. Therefore, findings from such samples might not be representative for modules in the field. It is therefore complicated to combine the different studies into common conclusions on PID effects.

In order to bridge this gap, we have developed a method that allows to conduct laboratory-style in-depth electrical and physical analysis on full-scale commercial modules.[11] This so-called coring and peeling approach leads to the formation of functioning small-scale cells from selected areas in a module. In an earlier study, the approach has been used to identify the changes in cell parameters on a PID-degraded commercial module that was known to be sensitive to high voltages.[11] This study revealed the relationship between local cell characteristics and full module performance, by using (among others) current–voltage, photoluminescence (PL) and illuminated lock-in thermography imaging. The lateral electrical differences within the modules could thus be identified. However, this study was focused on the relationship between the spatial electrical properties of the cells and modules. Further work was required in order to identify the physical degradation mechanism that occurred in the multilayer stack cell.

This paper follows a two-stage study to determine the relationship between the electrical performance of a cell and the changed composition of the layers and their interfaces. In the first stage, a second module from the same batch as studied in ref. [11] was PID-stressed. Coring and peeling then allowed the preparation of functioning small-scale cells from the degraded and non-degraded areas. These cells and their layers were studied in depth by both electrical and material analysis techniques and cell modelling to explain the PID. The samples studied at the first stage were consistently kept in the argon-filled glovebox. In the second stage, the samples were removed from the glovebox and stored under the ambient conditions. Some of the analysis techniques were repeated to understand further degradation under ambient conditions. This two-stage study allowed the identification of the local material changes, their correlation with performance losses and the proposal of a degradation mechanism.

2 | EXPERIMENTAL METHODS

The IEC 62804-1 test procedure was followed for a PID test. It dictates application of a bias voltage from an external power source between the grounded module frame and the solar cells through the shorted two connectors from the junction box. The commercial module investigated in this study is frameless; therefore, it was supported with metal bars, which were then connected to the power source with metal clamps. Current–voltage measurements were conducted, and electroluminescence images were taken both before and after the PID test.

A coring method was custom-developed for sample extraction from the defined areas. Devices consisting of four interconnected cells were prepared on extracted samples with active layers by scribing a defined area and forming silver contacts on the adjacent cells. Current–voltage measurements were conducted at room temperature under 1000 W/m^2 simulated AM1.5G illumination using a xenon lamp in a Neonsee solar simulator. Please refer to ref. [11] for detailed explanations of the PID test procedure and the sample preparation via coring and peeling.

A GreatEyes LumiSolarcell set-up with a silicon CCD camera was used for PL imaging. The samples were illuminated with two red LED lamps that have a peak emission at 660 nm. All images displayed in this paper were taken with a lens aperture of f/2.8 with integration time of 20 s. A black paper mask was used to cover the glass exposed from the scribes of the cored edge, which can otherwise saturate the luminescence image.

Current–voltage modelling was performed using the one-dimensional solar cell simulation program SCAPS (see Data S1). For the CdS and ZnO layers, the baseline parameters were used, while the thickness and composition of the absorber layer was measured with cross-sectional SEM and SIMS. Both dark and light curves were simulated. For the Mo/CIGS back-contact, flat band conditions were applied to minimize the barrier at the back.[12]

Depth profiles have been measured using an ION-TOF TOF-SIMS IV instrument operated in positive mode using 2 keV O_2^+ ions for sputtering.

3 | RESULTS AFTER PID

3.1 | Module performance and core selection

Current–voltage (*I*–*V*) curves of the field module measured before and after the PID tests are shown in Figure 1. The module power has dropped by 62%, which was mainly caused by 33% loss in open circuit voltage (V_{oc}) and 35% fill factor loss. On the other hand, the I_{sc} loss was only 12%. This agrees qualitatively with most of the literature on PID degradation of CIGS modules and minimodules and quantitatively with our previous study.[11]

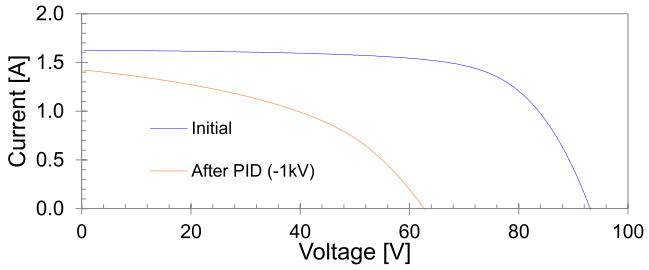

FIGURE 1 I–V curves of the module before and after the bias application of −1000 V for 48 h in a climate chamber at 85°C and 85% relative humidity (RH)

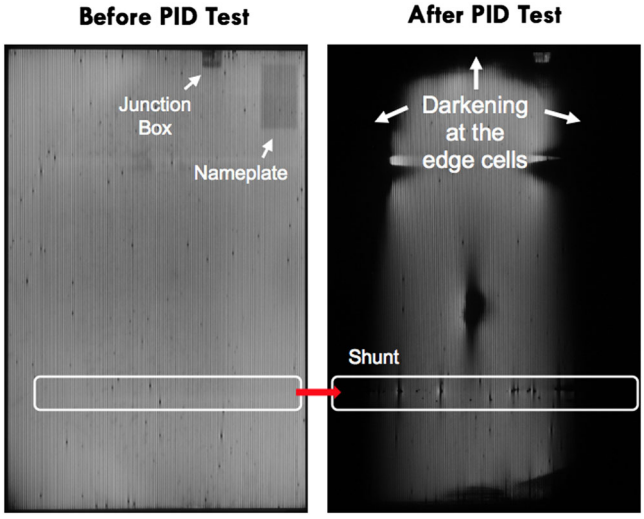

FIGURE 2 Electroluminescence (EL) images of a commercial CIGS PV module (1200 × 800 mm) taken before and after the PID test (bias applied: −1000 V for 48 h in a climate chamber of 85°C and 85% RH)

Figure 2 shows the electroluminescence images of the field module taken before and after the PID tests. We had similar observations to our previous study: The areas closer to the edge are non-luminescent and appear darker compared to the centre of the module. As explained in our previous study, this is due to non-uniform potential distribution upon PID stressing, which is higher closer to the edges as the potential is applied to the module via the clamps and the support at the edges, which is then spread over the module thanks to glass surface conductivity. Also, shunts have formed along a horizontal line after the PID test. The central part of the module still generates power; however, the edge cells have degraded.

3.2 | Post-mortem analysis of the extracted samples from the module via coring

Samples were selected from the areas of interest according to the EL image of the module after PID and were extracted from the module by coring. The samples were labelled and numbered as Dark and Reference representing degraded and non-degraded areas of the module, respectively. Figure 3 shows the PL images of the samples with their locations on the module (left). PL images are consistent with the module's EL image before coring. The Reference samples have higher PL

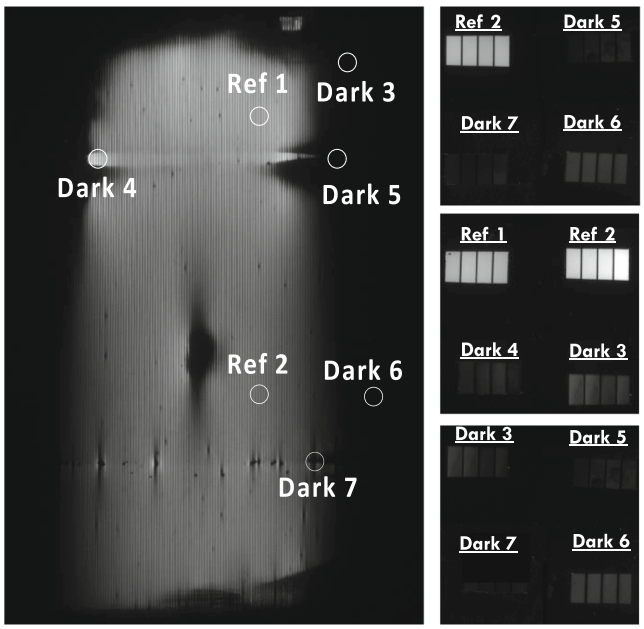

FIGURE 3 (Left) Electroluminescence image of the module after PID, indicating the locations of all analysed samples. (Right) The PL images are exhibited; the PL imaging was performed together for four samples in different combinations to enable a quantitative comparison.

intensity in comparison with Dark samples, in which less radiative recombination takes place. The PL was uniform across the interconnected cells for all samples.

3.2.1 | I–V measurements

The *I*–*V* curves of all samples are shown in Figure 4. Reference samples have a V_{oc} around 2.6 V, which matches well with the electrical performance of the cells prior to PID test suggesting that the coring and unpackaging processes do not create any harm. For the Dark samples that were extracted from degraded areas, a significant V_{oc} drop can be observed to values less than half of the reference samples. The degraded samples continue to show diode behaviour but a flattening of the curve in the fourth quadrant (power generation) that reduces the fill factor as well. At negative bias, the curves are flattening, and the shunt resistances R_{sh} have similar values. Thus, from the *I*–*V* curves, it appears that the reduced fill factor is not related to an increase in R_{sh}. There seems to be an increase in series resistance though, which could be related to the interconnection or the window layers.[13]

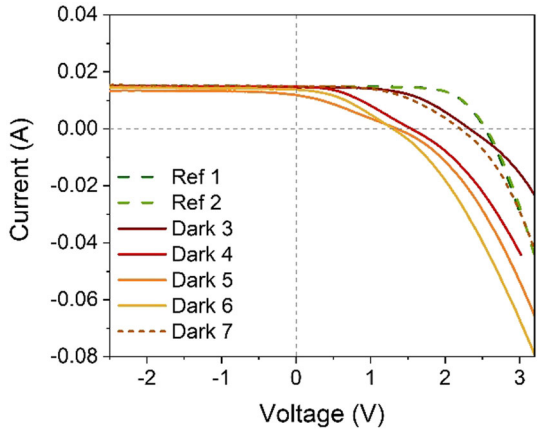

FIGURE 4 I–V curves of all samples that were extracted from both degraded and non-degraded areas. The curves are reported as total voltage for four interconnected cells versus current for comparison. All samples have the same area.

3.2.2 | SIMS

We have performed SIMS on two selected samples to investigate where alkali ions have migrated and accumulated to see whether this relates to the degradation of electrical properties. Figure 5 shows the alkali depth profiles, where the boundaries of the layers were defined based on the profiles of Zn, Cd, Ga, In and Mo. Sodium and potassium profiles of the Reference and Dark samples show a notable increase in their content in the absorber layer closer to buffer layer and a generally higher amount of alkali for the sample that was extracted from the degraded area. On the other hand, no increase of sodium or potassium was found in the ZnO layers of all samples. We can therefore assume that sodium migrated from the substrate glass, not the cover glass. We further investigated whether other metal ions such as Cr, Mn, Fe and Ni migrate upon PID stressing. The degraded and reference samples showed no significant differences in that respect (Figure 5, right).

4 | SCAPS MODELLING

After the PID treatment, it was found that the *I*–*V* curves of the 'Dark areas' are distorted (see Figure 4). For both the four interconnected cells and the single cells, the fill factor is reduced due to flattening of the curve in the fourth quadrant, and the V_{oc} is reduced. This distortion seen in the *I*–*V* curves, that is, the presence of multiple kinks at positive bias, is generally induced by unfavourable band alignment at the buffer/window and buffer/CIGS interfaces.[14] Yet, this mismatch in band alignment does not explain the large V_{oc} losses observed, which are generally due to increased recombination.

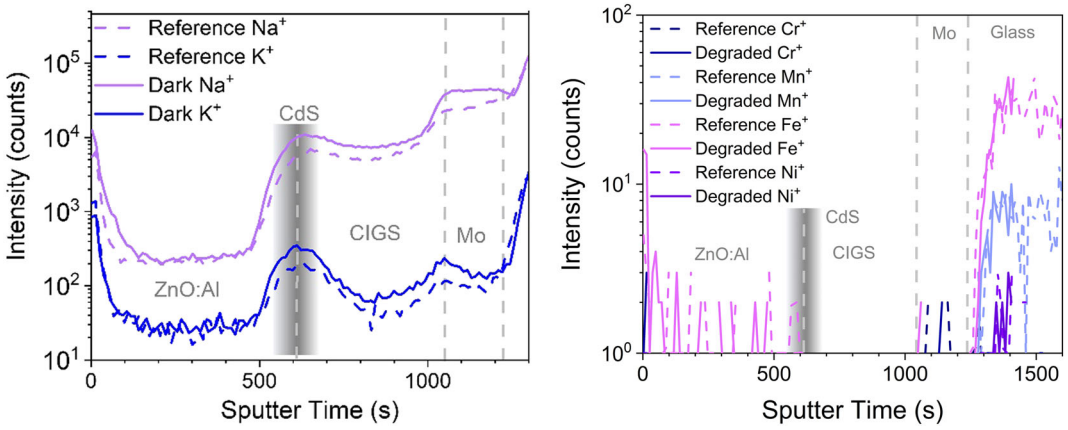

FIGURE 5 SIMS performed for selected reference and degraded sample demonstrates the sodium and potassium profile (left) and other metal profiles: Cr, Mn, Fe and Ni (right).

To further investigate this, the J_0 values were extracted from the *I*–*V* curves that were measured without illumination and are given in Table 1. For all the 'Dark' samples, it is found that the J_0 values increased compared to the reference indicating that recombination is also increased. The PL images of the Dark samples showed a drastically reduced yield (Figure 3, right). The PL yield is also a signature of the recombination processes in the bulk and at interfaces and lowering of the yield implies increased non-radiative recombination. Finally, it was observed that the J_{sc} losses are only marginal compared to the fill factor and V_{oc} losses.

To obtain more understanding in what might cause these changes upon PID of the 'Dark' samples, the stack was modelled using the 1D SCAPS simulation program.[15] The parameters used for the modelling can be found in Appendix S1. Defect densities in the bulk and at the CdS/CIGS and CdS/ZnO interfaces were varied, as well as the doping concentration in the CdS layer.

TABLE 1 Calculated J_0 and ideality factor for all samples

	J_0 (A/cm^2)	Ideality factor *n*
Ref 1	$3.82 \cdot 10^{-6}$	1.67
Ref 2	$3.97 \cdot 10^{-6}$	1.67
Dark 3	$9.82 \cdot 10^{-3}$	3.59
Dark 4	$2.13 \cdot 10^{-4}$	1.54
Dark 5	$1.24 \cdot 10^{-3}$	2.45
Dark 6	$9.18 \cdot 10^{-5}$	1.47
Dark 7	$7.03 \cdot 10^{-4}$	2.11

At first, various parameters were changed to find under which circumstances the kink and V_{oc} losses appear without reducing the current density too much. The results are presented in Figure 6. The first two graphs (A) and (B) present the effect that defects in the bulk have on the *I*–*V* curves. For acceptor defects (A), we find that the V_{oc} reduces significantly, while the fill factor and current density are only marginally affected. When acceptor defects are replaced by donor defects, also the current and fill factor are drastically reduced. This is presented in Figure 6B. As donor defects in the bulk reduced the current too much, it is unlikely these are responsible for the degradation seen in the 'Dark areas'. When acceptor defects are placed at the CdS/CIGS interface, it is found that both fill factor and V_{oc} reduces; only at very high concentrations also the current reduces (Figure 6C). The *I*–*V* curves show similar trend as that seen in the *I*–*V* curves of the 'Dark areas': flattening of the *I*–*V* curve in the 4th quadrant and V_{oc} losses. Further, defects at the CdS/ZnO interface were modelled, and it is found that these also cause a drastic distortion of the *I*–*V* curve. This is presented in Figure 6D. This distortion appears above V_{oc} though, and thus, interface defects at the CdS/ZnO interface are also unlikely to be the root cause of the degradation seen in the 'Dark areas'. Finally of the *I*–*V* curve as seen for CdS/CIGS

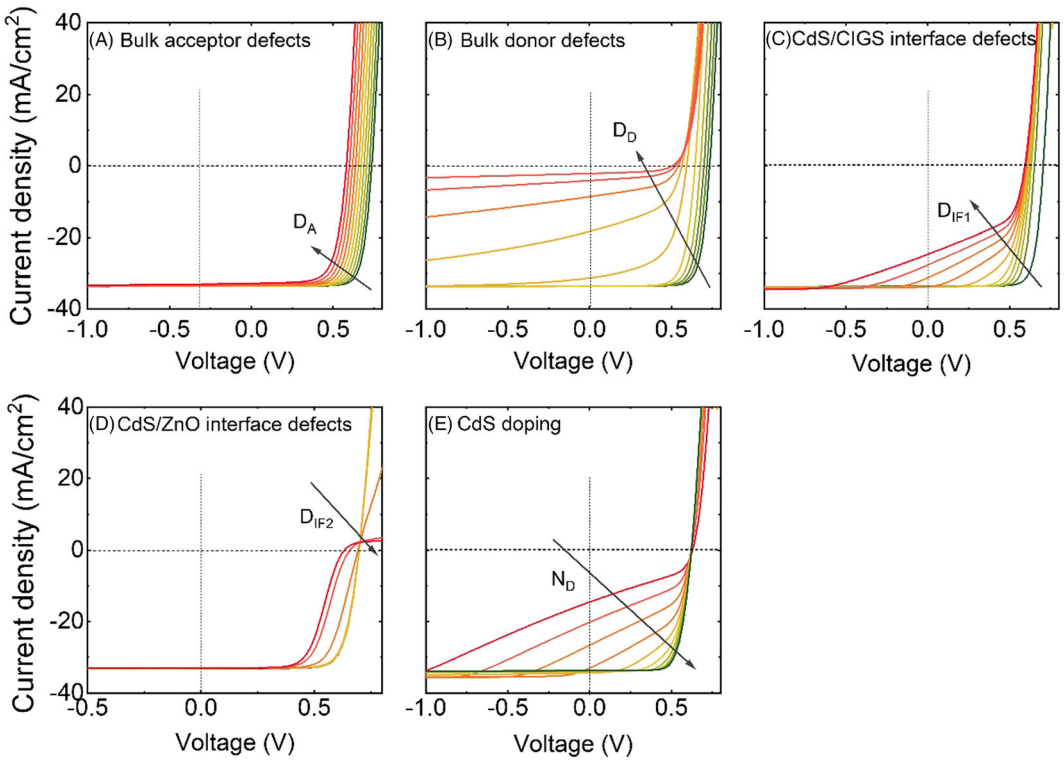

FIGURE 6 Simulated light current density–voltage curves with (A) bulk acceptor defect, (B) bulk donor defects, (C) acceptor defects at the CdS/CIGS interface, (D) acceptor defects at the CdS/ZnO interface and (E) CdS doping density with CdS/CIGS interface defects. The modelling parameters are given in Appendix S1. The arrows point in the direction of increasing value of the variable.

interface defects is enhanced when the doping in the CdS layer reduces. This is presented in Figure 6E. The interface defect concentration was kept constant, and only the donor concentration in the CdS layer was reduced. Thus, lowering of the donor concentration may also be part of the *I*–*V* curve distortion.

To assess the changes of the current that are measured without illumination, the curves of the simulated bulk acceptor defect, CdS/CIGS interface defects and reduced CdS doping are plotted as well. These curves are presented in Figure 7. It is found that the bulk defects have the largest impact on the curves, while the reduction of the CdS doping has only marginal impact. The impact of interface defects only lies somewhere between that of bulk and CdS doping.

In Figure 8A, the measured I–V curves without illumination are presented. The references follow a clear diode behaviour, where the series and shunt resistance can easily be distinguished from the diode. For the degraded cells, all these parts are merging, and a flattening of the curve at positive bias is seen. The distortion is thus much larger than what would be expected if the light *I*–*V* curve distortion is only due to interface defects (Figure 8B). The shunt—except for 'Dark 7'—is not increased as can be seen at negative bias; this was also concluded from the light curves in Figure 4. Therefore, the dark measurements suggest that acceptor defects play a large role in the degradation seen for the 'Dark areas'.

To confirm this hypothesis, acceptor bulk defects in combination with lower CdS doping were modelled and compared with CdS/CIGS interface defects. The light curves are presented in Figure 8B, and both light curves now show the flattening at positive bias and large V_{oc} losses, which is similar to the measured *I*–*V* curves of the 'Dark areas'. Thus, the measured light curves can be simulated using a combined effect of acceptor bulk defects and low concentration of CdS/interface with reduced CdS doping as well. The corresponding EQE spectra are presented in Appendix S1.

The *I*–*V* curves obtained without illumination though reveal a larger difference for the two defect types. When bulk defects are present, there is more flattening of the dark curve at positive bias (Figure 8C), which is closer to what is observed in the measurements (Figure 8A). We therefore hypothesize that bulk defects play a major role in the observed degradation as well. The

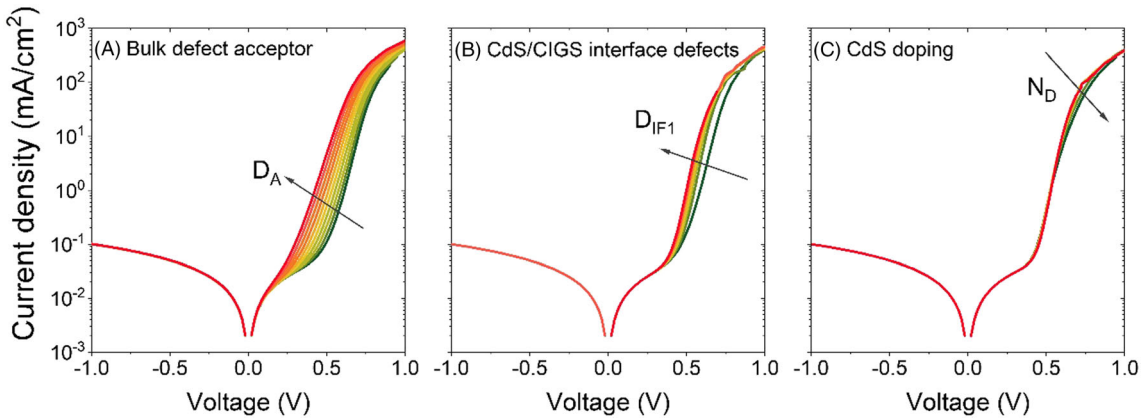

FIGURE 7 I–V curves of (A) bulk defect acceptor, (B) CdS/CIGS interface defects and (C) CdS doping obtained without illumination. The largest effect is seen for the bulk defects. The arrows point in the direction of increasing parameter value.

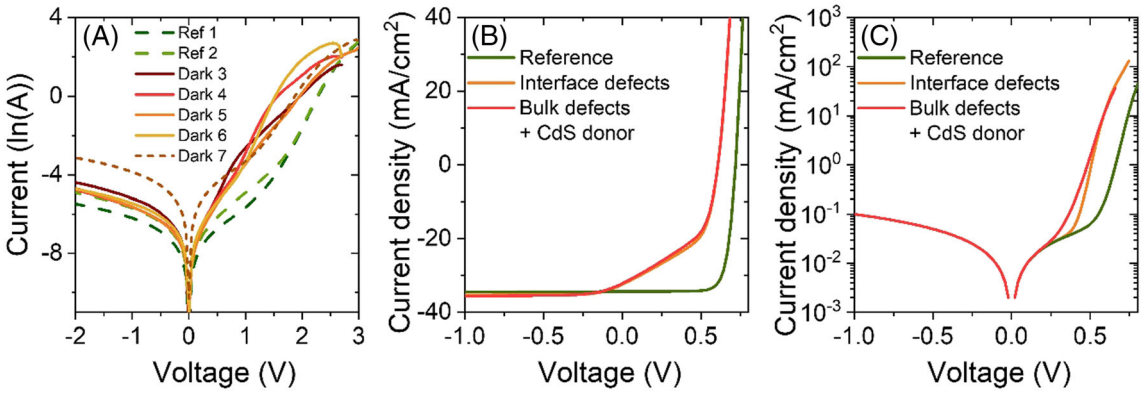

FIGURE 8 (A) I–V curves obtained without illumination. (B,C) Modelled I–V curves obtained under and without illumination with interface defects or bulk defects combined with reduced donor concentration in CdS layer

flattening of the *I*–*V* curve is due to CdS/CIGS interface defects though, which is enhanced by reduction of the doping in the CdS buffer layer.

It has to be noted that changes at the back contact were not modelled. It is known though that a resistive back contact also causes barrier behaviour in the *I*–*V* curve. This is seen, for instance, when dielectric passivation of the back contact with sub-optimal distance between the openings is applied or in the presence of a layer with lower valence band (rejection of holes).[16,17] The first option can be excluded as there is no dielectric layer present at the back. The second option would be visible in the SIMS profiles, as lowering of the valence band would require drastic changes in the composition. For instance, the ordered vacancy compound layer has a low valence band, but this layer has also low copper and gallium concentration. If such a layer is present at the back, it would be visible in the SIMS profile. As these changes were not seen in the SIMS profile, it is reasonable to assume that the observed *I*–*V* curve distortion is due to the changes at or in the buffer layer and the bulk and not the back-contact. Further IV measurements with changing illumination and temperature variations could help in securing the hypothesis. Yet, care needs to be taken for the relatively fast degradation of the 'Dark area' in ambient atmosphere.

The changes near the buffer layer and in the bulk may be induced by the presence of Na. The SIMS profiles indeed show a two- to threefold increase in Na amount in the CIGS and CdS layer compared to the reference. In general, Na is very important for appropriate compensation of the donor and acceptor defects in the absorber layer. However, this arrangement of the donor and acceptor defects is done during the cooling down phase, while in this experiment Na was added by applying a high electric field at a much lower temperature.[18,19] It is therefore possible that the added Na causes detrimental changes in the donor/acceptor concentration without re-establishing a more favourable equilibrium between these defects, which seems to happen when Na is added at elevated temperature during the cooling down phase. It is possible that the doping in CdS is also affected by the presence of Na, and thus, the doping might change as well upon increase of Na content.

5 | FURTHER DEGRADATION UNDER AMBIENT CONDITIONS

In the first stage of this study, which includes all measurements described above, the unpackaged cores were consistently kept in the glovebox, in case they were not measured. This meant that they were only exposed to argon for the vast majority of this time. After this, the samples were removed from the glovebox and stored under ambient conditions. This led to clear modification in the properties of the solar cells.

5.1 | J–V curves

The clearest indication for changed parameters can be found in the measured current–voltage curves. Figure 9 shows the curves directly after production and removal from the glovebox, as well as the curves after 102 and 192 days of exposure to ambient conditions. It should be mentioned that they were measured at different set-ups, but the differences between the curves is so strong that it is unlikely explained by set-up differences alone.

Figure 9 shows that all cells deteriorate when exposed to ambient conditions. The reference samples (A and B) show a relatively mild decrease in short-circuit current density (J_{sc}) and fill factor, while the V_{oc} remained constant. For the PID-degraded samples (C and D), the

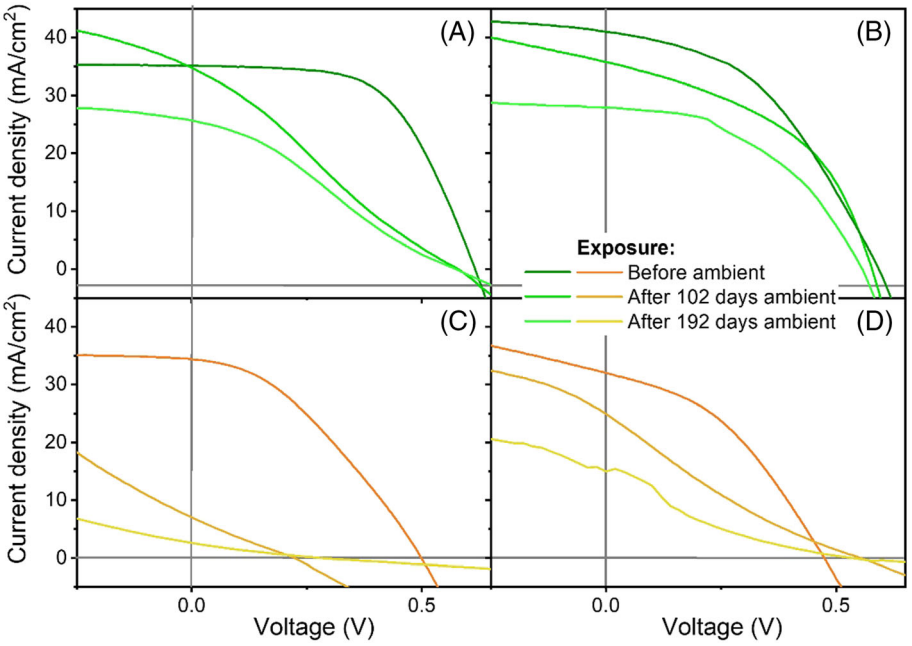

FIGURE 9 Current density–voltage measurements on small single cells (about 10–16 mm^2) executed directly after cell production and removal from the glovebox, after ambient exposure for 102 days and after ambient exposure for 192 days. (A) and (B) are positions on 'Reference 1', while (C) and (D) could be found on 'Dark 5'.

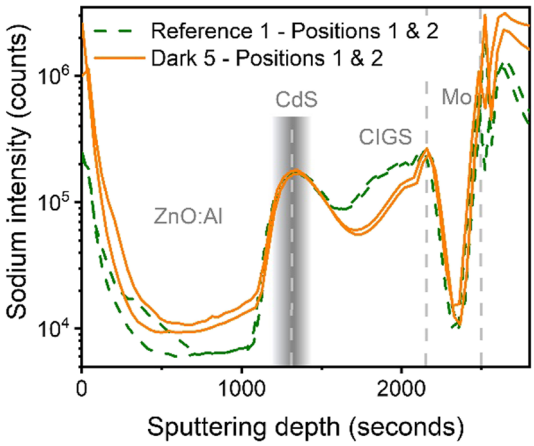

FIGURE 10 Sodium SIMS measurements as a function of depth of positions in a dark ('Dark 5', orange line) and a reference ('Reference 1') sample. These samples have been exposed to ambient conditions for 192 days.

effect was much more severe: A relatively strong decrease in J_{sc} was observed, while the fill factor decreased to values below 25%. This indicates that the devices no longer performed as real diodes. It appears that cored PID-degraded devices are much more sensitive to ambient exposure than cells from the less affected (reference) regions.

5.2 | SIMS

In order to learn more about the cause for the reduced power output after exposure to ambient environment, SIMS measurements were taken. It should be noted that they were taken on different samples and with a different tool than the results as described in Section 3.2.2. Any differences and similarities should therefore be considered with care. We can however clearly recognize trends between the samples measured in this series.

First of all, no differences were observed for the exposed reference and dark samples in the depth spectra of Si, Mg, Mo, Se, Cu, In, Ga, Cd, Zn, Al, O, OH, S, Ni, Cl, Ca, C and B. For the sodium spectra, on the other hand, clear differences were observed (Figure 10). Actually, the sodium was lower in the 'dark' positions in the bottom half of the CIGS absorber for the 'Dark 5' sample compared to the reference. This is in contrast to earlier findings in ref. [11] and SIMS measurements shortly after coring as presented in Section 3.2.2 (Figure 5). Additionally, the sodium content is higher in the ZnO:Al front contact, especially near the ZnO:Al/air interface.

The sodium concentration in the CIGS layer of the Dark samples shows a striking steepness. This is indicative of out-diffusion of sodium, upwards into the ZnO:Al layer. Indeed, an enhanced sodium concentration (and a gradient) can also be seen in that region. The steepness is distinctly higher than the other SIMS analyses in Figures 5 and 10 show. Perhaps the sodium is mobile at room temperature and diffuses further over time towards a lower-concentration region (the ZnO). As a result, the sodium concentration in the ZnO region now rises, which was not observed earlier in cored samples from this CIGS technology. The diffusivity in the reference sample appears much lower, as a large sodium concentration gradient is maintained. It appears from this SIMS profile that the PID stress has somehow mobilized sodium or created physical paths for enhanced diffusion.

These results show that PID leads to direct but also delayed consequences. While the direct consequences were clearly identified in ref. [11] and earlier SIMS in Section 3.2.2, identification and interpretation of the delayed effects in ambient is more complicated. It is likely that ions or compounds from the atmosphere play a role. In earlier work in ref. [20], it was shown that CIGS solar cells can be very stable under illumination and elevated temperature as long as humidity is absent. Moreover, sodium is known to have a key role in degradation behaviour, in combination with humidity, and for some mechanisms, CO_2.[21,22] It is therefore likely that the migration of sodium within the solar cell stack itself was enhanced due to water (and possible CO_2) ingression after exposure to ambient conditions. This might explain the rapid degradation under these conditions.

It should be mentioned that the 'reference' cells also degraded over time in ambient storage. Since no exact copies from a non-PID-prone module exist, no solid comparison can be made about the degradation rate and mechanisms under ambient conditions. However, based on earlier experiments, it seems that the loss in fill factor and especially J_{sc} are faster than for average CIGS cells, which did not originate from a PID-prone module. This might indicate that also some chemical changes, like mild sodium migration, occurred in the 'reference' cells during (or after) the PID experiment, which might have developed further under ambient conditions. Only after their interaction with humidity (and CO_2) this might have strongly affected the *I*–*V* parameters.

6 | DISCUSSION

The data in this article reconfirm observations presented in ref. [11] that part of the CIGS module is severely damaged after PID while the rest, mostly the centre of the module, seems rather unaffected. The electroluminescence images clearly show this contrast. Coring samples taken from dark and bright regions confirm distinct differences in their *I*–*V* performance.

On module level, PID leads to 62% power loss, which is mainly caused by 33% V_{oc} loss and 35% fill factor loss. The long cells in this module (stretching over its full length) make it difficult to relate this module performance to the performance of the cored cells in a quantitative sense. The dark cells show distorted *I*–*V* curves. Significant V_{oc} drop can be observed in these samples as well as fill factor losses. The degraded samples continue to show diode behaviour with similar R_{sh} values in comparison to reference samples.

Further *I*–*V* analysis of the damaged cells supported by SCAPS simulations shows that bulk defects, and to a lesser extent interface defects, are responsible for the distortion of the *I*–*V* curves. A reduced CdS doping may also play a role.

From SIMS, it can be concluded that most elements stay in place during PID, except Na. Sodium piles up in the absorber and in the Mo back contact; the concentration almost doubles in those regions. Given that the concentration of sodium has been optimized in the produced modules, it can only be expected that a change in Na concentration leads to performance loss.[23] It is likely that these elevated Na concentrations are the cause of the bulk defects mentioned above. The SIMS data further clarify that no other metallic species migrate significantly, except potassium, which might be migrating in a manner similar to sodium.

Altogether, from this work it can be concluded that PID leads to localised cell damage. Our results strongly suggest that additional sodium migration into the absorber lead to a local, severe loss of V_{oc}, fill factor and J_{sc}, affecting the module performance as a whole. No evidence was found that other elements play a role, as no change was observed in the SIMS profiles of these elements.

We see two possible reasons why PID damage concentrates at the module edges. The first (as discussed in ref. [11]) is that leakage currents may lead to local build-up of electrostatic charge, causing electric fields to concentrate. Such creepage-like effects can take place along surfaces and interfaces; penetration of the externally applied high voltage into the module via the edges is a possibility. A second possible explanation is that although cells receive similar PID stress, the effect at the module edges is stronger because ambient species (water, CO_2 or other) penetrate the module from the edges inwards to attack the stressed cells. It was earlier shown that alkali metals in the CIGS absorber layer cause ingression of water into the absorber layer.[24] This could partly explain the findings of this study, in which PID stressed samples with more alkali degrade faster in air.

A further conclusion from this work is that decapsulated CIGS cells degrade under ambient conditions. PID-damaged cells degrade much faster than unaffected parts of the module. This limits the possibilities for failure analysis by means of decapsulation. This finding may also imply that PID-stressed cells degrade faster in case of hermeticity problems (which are generally more significant in smaller-area samples). PID mitigation could then be achieved either by electric field reduction or by improvement of the long-term hermeticity of CIGS modules.[13]

7 | CONCLUSIONS

Recent work on cored CIGS samples established a direct correspondence between the PID-induced phenomena on module level and on cell level, and the present work strengthens this correspondence. Cells extracted from areas with low electroluminescence show dramatically deteriorated current–voltage characteristics, while reference cells from the brighter parts of the module still perform well. SIMS analysis, SCAPS-based modelling and analysis of the current–voltage characteristics of cored module samples show a redistribution of sodium, and perhaps potassium, after PID stressing, accompanied with a stronger manifestation of bulk defects and interface defects. Other impurities do not seem to redistribute in the layer stack. It was also found that cells from the areas with low electroluminescence degrade strongly in ambient conditions and again Na profiles show large changes compared to the lesser affected cells. The control of alkali ion redistribution and humidity ingress therefore appear to be the most effective mitigation approaches for potential-induced damage in CIGS photovoltaic modules.

ACKNOWLEDGEMENTS

We would like to acknowledge the Early Research Program 'Sustainability & Reliability for solar and other (opto-)electronic thin-film devices' (STAR) from TNO for partial funding of this work. Moreover, this work is part of the Solar.Eranet project Performance and Electroluminescence Analysis on Reliability and Lifetime of Thin-Film Photovoltaics (PEARL) and supported in Germany by a grant of the BMWi under project number 0324193B and in the Netherlands under project number TEUE116203. We also would like to thank Joran van den Berg, Klaas Bakker, Gonzalo Ott Cruz and Henk Steijvers for their help in the laboratory.

DATA AVAILABILITY STATEMENT

The data that supports the findings of this study are available in the supplementary material of this article

REFERENCES

1. Aghaei M, Fairbrother A, Gok A, et al. Review of degradation and failure phenomena in photovoltaic modules. *Renew Sustain Energy Rev*. 2022;159:112160. doi:10.1016/j.rser.2022.112160
2. Luo W, Khoo YS, Hacke P, et al. Potential-induced degradation in photovoltaic modules: a critical review. *Energ Environ Sci*. 2017;10(1):43-68. doi:10.1039/C6EE02271E
3. Voswinckel S, Mikolajick T, Wesselak V. Influence of the active leakage current pathway on the potential induced degradation of CIGS thin film solar modules. *Solar Energy*. 2020;197:455-461. doi:10.1016/j.solener.2019.12.078
4. Yamaguchi S, Jonai S, Hara K, et al. Potential-induced degradation of Cu (In,Ga)Se_2 photovoltaic modules. *Jpn J Appl Phys*. 2015;54(8):697-708.
5. Yilmaz P, Schmitz J, Theelen M. Potential Induced degradation of CIGS PV systems: a literature review. *Renew Sustain Energy Rev*. 2022;154:111819. doi:10.1016/j.rser.2021.111819
6. Fjällstrom V, Salomé PMP, Hultqvist A, et al. Potential-induced degradation of $CuIn_{1-x}Ga_xSe_2$. *IEEE J Photovolt*. 2013;3:1090-1094.
7. Muzzillo CP, Glynn S, Hacke P, et al. Potential-induced degradation of Cu(In,Ga)Se_2 solar cells: alkali metal drift and diffusion effects. *IEEE J Photovolt*. 2018;8(5):1337-1342. doi:10.1109/JPHOTOV.2018.2858549
8. Naumann V, Lausch D, Hähnel A, et al. Explanation of potential-induced degradation of the shunting type by Na decoration of stacking faults in Si solar cells. *Sol Energy Mater Sol Cells*. 2014;120:383-389. doi:10.1016/j.solmat.2013.06.015
9. Swanson R, Cudzinovic M, DeCeuster D, et al. The surface polarization effect in high-efficiency silicon solar cells. *Proceedings of 15th International Photovoltaic Solar Energy Conference and Exhibition*, 2005; 410.
10. Xiao C, Jiang C, Harvey SP, et al. In-situ microscopy characterization of Cu (In,Ga)Se_2 potential-induced degradation. *Proceedings of 46th IEEE Photovoltaic Specialists Conference*, 2019; 2342–2345.
11. Yilmaz P, Aninat R, Ott Cruz G, Weber T, Schmitz J, Theelen M. Post-mortem analysis of a commercial copper indium diselenide (CIGS)

photovoltaic module after potential induced degradation. *Prog Photovolt: Res Appl*. 2022;30(6):640-647. doi:10.1002/pip.3538
12. Frisk C, Platzer-Bjorkman C, Olsson J, et al. Optimizing Ga-profiles for highly efficient Cu (In, Ga)Se_2 thin film solar cells in simple and complex defect models. *J Phys D Appl Phys*. 2014;47:485104.
13. Theelen M, Daume F. Stability of Cu(In,Ga)Se_2 solar cells: a literature review. *Solar Energy*. 2016;133:586-627. doi:10.1016/j.solener.2016.04.010
14. Sozzi G, Troni F, Menozzi R. On the combined effects of window/buffer and buffer/absorber conduction-band offsets, buffer thickness and doping on thin-film solar cell performance. *Sol Energy Mater Sol Cells*. 2014;121:126-136. doi:10.1016/j.solmat.2013.10.037
15. Burgelman M, Nollet P, Degrave S. Modelling polycrystalline semiconductor solar cells. *Thin Solid Films*. 2000;361-362:527-532. doi:10.1016/S0040-6090(99)00825-1
16. Ledinek D, Donzel-Gargand O, Skold M, Keller J, Edoff M. Effect of different Na supply methods on thin Cu(In,Ga)Se_2 solar cells with Al2O3 rear passivation layers. *Sol Energy Mater Sol Cells*. 2018;187:160-169. doi:10.1016/j.solmat.2018.07.017
17. Li J, Deng B, Zhu H, et al. Rear interface modification for efficient Cu(In,Ga)Se_2 solar cells processed with metallic precursors and low-cost Se vapor. *Sol Energy Mater Sol Cells*. 2018;186:243-253. doi:10.1016/j.solmat.2018.06.052
18. Miredin C, Raghuwanshi O, Wuerz M, Sadewasser R. Grain boundaries in Cu(In, Ga)Se_2: a review of composition–electronic property relationships by atom probe tomography and correlative microscopy. *Adv Funct Mater*. 2021;31(41):2103119. doi:10.1002/adfm.202103119
19. Yuan ZK, Chen S, Xie Y, et al. Na-diffusion enhanced p-type conductivity in Cu(In,Ga)Se_2: a new mechanism for efficient doping in semiconductors. *Adv Energy Mater*. 2016;6(24):1601191. doi:10.1002/aenm.201601191
20. Theelen M, Beyeler K, Steijvers H, Barreau N. Stability of CIGS solar cells under illumination with damp heat and dry heat: a comparison. *Mater Sol Cells*. 2017;166:262-268. doi:10.1016/j.solmat.2016.12.039
21. Theelen M, Hans V, Barreau N, Steijvers H, Vroon Z, Zeman M. The impact of sodium and potassium on the degradation of CIGS solar cells. *Prog Photovolt: Res Appl*. 2015;23(5):537-545. doi:10.1002/pip.2610
22. Theelen M, Foster C, Barreau N, Steijvers H, Vroon Z, Zeman M. Influence of atmospheric species water, oxygen, nitrogen and carbon dioxide on the degradation of CIGS solar cells. *Sol Energy Mater Sol Cells*. 2015;141:49-56. doi:10.1016/j.solmat.2015.05.019
23. Kessler F, Rudmann D. Technological aspects of flexible CIGS solar cells and modules. *Solar Energy*. 2004;77(6):685-695. doi:10.1016/j.solener.2004.04.010
24. Kohl T, Rivas NA, de Wild J, et al. Inclusion of water in Cu(In,Ga)Se_2 absorber material during accelerated lifetime testing. *ACS Appl Energy Mater*. 2020;3(6):5120-5125. doi:10.1021/acsaem.0c00610

SUPPORTING INFORMATION

Additional supporting information can be found online in the Supporting Information section at the end of this article.

How to cite this article: Yilmaz P, de Wild J, Aninat R, et al. In-depth analysis of potential-induced degradation in a commercial CIGS PV module. *Prog Photovolt Res Appl*. 2023;31(6):627-636. doi:10.1002/pip.3670